DOI: 10.1002/ejic.200601144

Synthesis and Study of the Crystallographic and Magnetic Structure of $HoFeMnO_5$

Angel Muñoz,*[a] José A. Alonso,[b] María J. Martínez-Lope,[b] and José L. Martínez[b]

Keywords: Ferrimagnetic structure / Superexchange interactions / Neutron diffraction / High oxygen pressure

A new oxide of stoichiometry $HoFeMnO_5$ has been obtained by replacing Mn^{3+} cations by Fe^{3+} in the parent oxide $HoMn_2O_5$. The crystallographic and magnetic structures have been analyzed by neutron powder diffraction (NPD), which complements susceptibility and magnetization measurements. $HoFeMnO_5$ is orthorhombic, belonging to the *Pbam* space group like the parent compound. The crystal structure contains infinite chains of edge-sharing $Mn^{4+}O_6$ octahedra, interconnected by dimer units of $Fe^{3+}O_5$ square pyramids. In comparison with $HoMn_2O_5$, containing elongated $Mn^{3+}O_6$ pyramids, the $Fe^{3+}O_5$ units are flattened. The magnetization measurements show that $HoFeMnO_5$ presents a long-range magnetic order below $T_C \approx 153$ K. An NPD study shows that $HoFeMnO_5$ adopts a collinear ferrimagnetic structure: each of the Mn^{4+} and Fe^{3+} sublattices are ferromagnetically coupled, and the coupling between the two sublattices is antiferromagnetic; the magnetic moments are oriented along the *c* direction. The Ho^{3+} cations also order below T_C, but with a very small magnetic moment; the Ho^{3+} moments are parallel to the Fe^{3+} magnetic sublattice. At $T = 2.7$ K, the ordered magnetic moments for the Mn^{4+}, Fe^{3+} and Ho^{3+} ions are 1.31(6), 3.20(10) and 0.36(7) μ_B, respectively. In comparison with $ErFeMnO_5$, where Er^{3+} cations are fully ordered at low temperatures, in $HoFeMnO_5$ there is a frustration concerning the long-range order of the Ho^{3+} cations, which remain virtually paramagnetic over the whole temperature range.

Introduction

In the last years, the interest in some rare-earth manganese oxide families such as RMn_2O_5 (R = rare earth, Y or Bi) has been revitalized, as different studies have shown a strong coupling between magnetism and ferroelectricity, also in the oxides that are in the select club of magneto-ferroelectric materials.[1–6] For instance, in $TbMn_2O_5$, the application of an oscillating magnetic field can reverse the direction of the electrical polarization.[2,3,6] As it has been demonstrated for $(Tb,Dy,Ho)Mn_2O_5$,[5,6] an external magnetic field also gives rise to a strong increase in the dielectric constant near the order temperature T_N.

RMn_2O_5 compounds crystallize in an orthorhombic crystallographic structure having space group *Pbam*. The 4*f* and 4*h* sites are occupied by the Mn^{4+} and Mn^{3+} cations, respectively.[7–11] The structure contains infinite chains of edge-sharing $Mn^{4+}O_6$ octahedra arranged along the *c* axis; the chains are corner-linked by pairs of $Mn^{3+}O_5$ edge-sharing pyramids. Below T_N, in the temperature interval 39–45 K, most of the RMn_2O_5 compounds become magnetically ordered according to an incommensurate magnetic structure[12,13] defined by the propagation vector $\mathbf{k} = (k_x,0,k_z)$, with $k_x \approx 0.5$. A few compounds of this family present a commensurate magnetic structure such as $BiMn_2O_5$, $\mathbf{k} = (1/2,0,1/2)$,[14] and $LaMn_2O_5$, $\mathbf{k} = (0,0,1/2)$.[15] A few degrees below T_N, the onset of a ferroelectric transition takes place, with the polarization vector **P** oriented along the *b* axis. Very recently, it has been reported that $(Ho,Tb,Er,Y)Mn_2O_5$ presents a magnetic transition to a commensurate structure at the ferroelectric transition temperature T_C. Furthermore, on decreasing temperature, another magnetic transition to an incommensurate structure happens, which coincides with an anomaly in the dielectric constant.[4,16–19]

Recently, a new series of rare-earth manganese oxides has been derived from RMn_2O_5 by replacing Mn^{3+} by Fe^{3+} cations. The crystallographic structure and the magnetic behaviour of $YFeMnO_5$ and $ErFeMnO_5$ have already been reported.[20,21] The sample preparation requires a high-oxygen-pressure treatment, in order to stabilize Mn^{4+} cations into the crystal structure. These novel $RFeMnO_5$ compounds keep the orthorhombic structure (space group *Pbam*) of the parent RMn_2O_5 oxides. However, important changes are observed in the magnetic behaviour, as both $YFeMnO_5$ and $ErFeMnO_5$ display ferrimagnetic behaviour below $T_C \approx 165$ K. The magnetic moments of the Mn^{4+} and Fe^{3+} cations are antiferromagnetically coupled along the *c* direction.

---

[a] Dpto. de Física Aplicada, EPS, Universidad Carlos III, Avda. Universidad 30, 28911, Leganés-Madrid, Spain
E-mail: angel.munoz@uc3m.es
[b] Instituto de Ciencia de Materiales de Madrid, CSIC, 28049, Cantoblanco-Madrid, Spain

In this paper we describe a new phase of this family, $HoFeMnO_5$, for which we report the crystallographic structure and the magnetic properties, analyzed by neutron powder diffraction (NPD); the magnetic behaviour is also investigated by macroscopic magnetization measurements.

Results

Sample Preparation

Stoichiometric amounts of analytical grade Ho_2O_3, $FeC_2O_4·2H_2O$ and $MnCO_3$ were dissolved in citric acid; the solvent was slowly evaporated, and the obtained organic resin was dried at 120 °C and slowly decomposed at temperatures up to 600 °C in air. High-oxygen-pressure treatments were performed in a VAS furnace. About 2 g of the precursor powder were placed in a gold can during the oxygenation process. The sample was slowly heated up to 900 °C at a final pressure of 200 bar and held at this temperature for 12 h. The product was finally cooled, under pressure, at 300 °C/h, down to room temperature. Finally, the oxygen pressure was slowly released.

Magnetic Susceptibility and Magnetization

The magnetic measurements were performed in a commercial SQUID magnetometer from Quantum Design. The dc magnetic susceptibility was measured both in zero-field cooling (ZFC) and field cooling (FC) conditions in the temperature intervals $1.8 < T < 400$ K and $1.8 < T < 328$ K, respectively, under a magnetic field of 1 kOe. Ac magnetic susceptibility measurements were also carried out in the temperature range 50–250 K, the frequencies of the transversal oscillating magnetic field being 0.32, 7, 33, 321 and 997 Hz. As regards the isothermal magnetization curves, different hysteresis cycles were obtained at $T = 3$, 50 and 225 K for a magnetic field ranging from –50 kOe to 50 kOe.

Neutron Diffraction Data

The NPD experiments were carried out at the Institut Laue-Langevin, Grenoble (France). For the study of the crystallographic structure, two patterns, one at room temperature and one at 10 K were collected with the high-resolution D2B diffractometer, at a wavelength of 1.594 Å. For the magnetic structure resolution and the study of its thermal evolution, a set of NPD patterns were acquired with the high-flux D20 diffractometer at $\lambda = 2.418$ Å and in the temperature interval $2.7 < T < 267$ K. The refinement of the different NPD diagrams was performed by the Rietveld method[22] with the Fullprof program.[23] A pseudo-Voigt function was used for the simulation of the profile of the Bragg peaks and a fifth-degree polynomial function was used for the fitting of the background. The coherent scattering lengths for Ho, Fe, Mn and O were 8.01, 9.45, –3.73 and 5.803 fm, respectively.

Results of Magnetic Measurements

The ZFC and FC curves of the dc susceptibility are presented in Figure 1. Both curves coincide at high temperature, but below $T_C \approx 153$ K the two curves split at the onset of a magnetic ordering process. Below T_C, the ZFC susceptibility curve steadily increases and exhibits a maximum at $T = 100$ K, which suggests the presence of antiferromagnetic interactions, and then a minimum at around 50 K, where a new change in the slope of the ZFC susceptibility indicates the presence of a remnant magnetization. The FC susceptibility curve continuously increases below T_C, also displaying a change in the slope at around 50 K. In the isothermal magnetization curves represented in Figure 2, a narrow hysteresis loop is observed at $T = 50$ K and $T = 2$ K with a remnant magnetization of 0.11 and 0.32 μ_B per formula, respectively. A maximum magnetization of 6.5 μ_B/f.u. is reached for the maximum applied field of 5 T. The presence of a remnant magnetization is in good agreement with the thermal behaviour of the dc susceptibility below T_C and with the ferrimagnetic order determined from the neutron diffraction data. At $T = 225$ K, the isothermal magnetization curve presents linear behaviour, as it corresponds to a paramagnetic state.

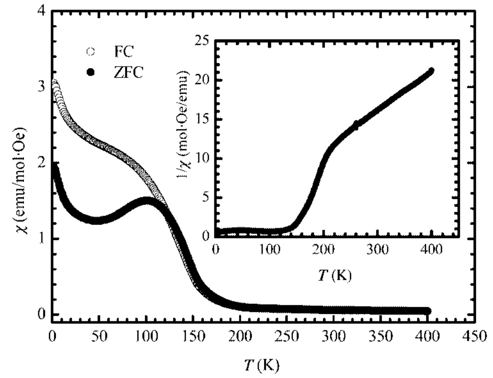

Figure 1. Thermal evolution of the field cooling (FC) and zero-field cooling (ZFC) dc susceptibility. Inset: inverse of the susceptibility (ZFC data).

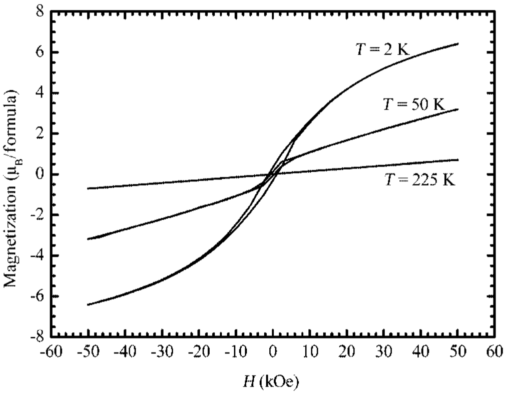

Figure 2. Magnetization vs. magnetic field isotherms at $T = 2$, 50 and 225 K.

As it can be seen in the inset of Figure 1, the inverse of the susceptibility shows linear behaviour at high temperature; in the temperature interval $263 < T < 395$ K, the reciprocal susceptibility is fitted to a Curie–Weiss law, yielding a paramagnetic temperature Θ_P = –28.5(5) K and an effective paramagnetic moment of 12.16(1) μ_B/f.u. The theoretical effective magnetic moment can be estimated by considering the expression $\mu_{eff} = [\mu_B(Mn^{4+})^2 + \mu_B(Fe^{3+})^2 + \mu_B(Ho^{3+})^2]^{1/2}$; the effective magnetic moments for spin-only Mn^{4+}, high-spin Fe^{3+} and Ho^{3+} ($^5I_8$ ground state configuration) are 3.87, 5.92 and 10.60 μ_B, respectively, which implies an effective magnetic moment of 12.74 μ_B, in good agreement with the experimental value.

The thermal evolution of the ac susceptibility is shown in Figure 3 for temperatures ranging from 50 to 250 K at different frequencies. χ' and χ'' represent the real (in-phase) and imaginary (out-of-phase) components of the susceptibility, respectively. Both χ' and χ'' present only one maximum at around the long-range ordering temperature $T_C \approx$ 153 K, and the height of the peak decreases with increasing frequency; in both cases, the position of the maximum does not seem to shift upon varying the frequency.

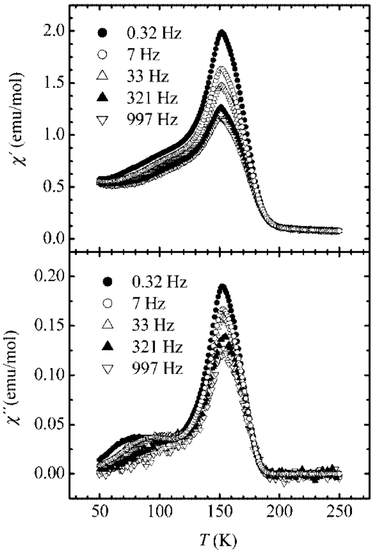

Figure 3. Thermal evolution of the real and imaginary parts of the ac susceptibility.

Crystallographic Structure from Neutron Powder Diffraction

For the refinement of the crystallographic structure, two high-resolution NPD patterns, one acquired at room temperature and the other at T = 10 K, with λ = 1.594 Å were used. In the refinement carried out with the room temperature NPD pattern, all the Bragg peaks of the diagram could be indexed in the orthorhombic space group *Pbam*. Firstly, it was assumed that the Mn and Fe atoms occupy the 4*f* (*0*,1/2,*z*) and 4*h* (*x*,*y*,1/2) sites, respectively; however, a better fit was obtained if a certain anti-site disorder was allowed between Mn and Fe atoms. The lattice parameters obtained in the refinement and the corresponding discrepancy factors are shown in Table 1. In Table 2, the atomic positions and the occupancy of the Mn/Fe cations are presented. At room temperature, the 4*f* site is occupied at 94(2)% by the Mn atoms [6(2)% of Fe atoms]; in contrast, in the 4*h* site the disorder is slightly higher, since it is occupied at 86(2)% and 14(2)% by Fe and Mn atoms, respectively. Since a high oxygen pressure was necessary for the sample preparation, the possible deficiency in oxygen has also been checked by refining the oxygen occupancy at room temperature. As it is shown in Table 2, a small oxygen deficiency seems to ex-

Table 1. Lattice parameters and reliability factors of the Rietveld refinements from NPD data with λ = 1.594 Å.

	Room temp.	T = 10 K
a (Å)	7.2793(4)	7.2652(5)
b (Å)	8.5060(4)	8.4938(5)
c (Å)	5.6921(3)	5.6851(3)
Vol. (Å^3)	352.44(3)	350.82(4)
R_P (%)	2.7	3.1
R_{wp} (%)	3.4	4.0
R_B (%)	6.5	8.0
χ^2	1.4	1.8

Table 2. Atomic parameters after the refinement of the crystallographic structure from NPD data with λ = 1.594 Å. Sites: Ho and O2 in 4*g* (*x*,*y*,0), Mn in 4*f* (0,1/2,*z*), Fe and O3 in 4*h* (*x*,*y*,1/2), O1 in 4*e* (0,0,*z*) and O4 in 8*i* (*x*,*y*,*z*).

		Room temp.	T = 10 K
Ho	x	0.1353(5)	0.1350(6)
	y	0.1704(4)	0.1701(4)
	B (Å^2)	0.48(6)	0.19(5)
Mn/Fe′	z	0.264(2)	0.272(2)
	B (Å^2)	0.3(2)	0.19(5)
	Occup. (%)	0.94(2)/0.06(2)	0.98(2)/0.02(2)
Fe/Mn′	x	0.3892(4)	0.3905(5)
	y	0.3543(4)	0.3546(4)
	B (Å^2)	0.32(8)	019(5)
	Occup. (%)	0.86(2)/0.14(2)	0.88(2)/0.12(2)
O1	z	0.2660(13)	0.259(2)
	B (Å^2)	0.44(8)	0.78(4)
	Occup. (%)	92(2)	92(2)
O2	x	0.1598(8)	0.1623(8)
	z	0.4449(5)	0.4461(6)
	B (Å^2)	1.13(10)	0.78(4)
	Occup. (%)	99(2)	99(2)
O3	x	0.1465(8)	0.1456(9)
	y	0.4322(6)	0.4349(6)
	B (Å^2)	0.99(9)	0.78(4)
	Occup. (%)	92(2)	92(2)
O4	x	0.3939(4)	0.3932(5)
	y	0.2046(4)	0.2057(4)
	z	0.2413(6)	0.2397(7)
	B (Å^2)	1.07(6)	0.78(4)
	Occup. (%)	96(2)	96(2)

ist, which is as high as 8(2)% for the O1 and O3 atoms. The crystallographic formula refined from NPD data is HoFe$_{0.92(2)}$Mn$_{1.08(2)}$O$_{4.74(10)}$, yielding a slightly Mn-rich compound with respect to the nominal stoichiometry. The most characteristic interatomic distances and bond angles are presented in Table 3. The good agreement between the experimental and calculated NPD patterns in the final Rietveld fit can be observed in Figure 4a.

Table 3. Selected interatomic distances (Å) and bond angles (°).

	Room temp.	T = 10 K
Mn–O2 (× 2)	1.955(11)	1.999(9)
Mn–O3 (× 2)	1.811(11)	1.761(9)
Mn–O4 (× 2)	1.908(3)	1.921(4)
<Mn–O>	1.891(9)	1.894(7)
Fe–O1 (× 2)	1.9906(6)	2.000(9)
Fe–O3	1.887(7)	1.904(7)
Fe–O4 (× 2)	1.947(4)	1.947(4)
<Fe–O>	1.952(5)	1.968(7)
Ho···O1 (× 2)	2.316(6)	2.284(7)
Ho···O2	2.341(6)	2.353(6)
Ho···O2	2.430(6)	2.406(7)
Ho···O4 (× 2)	2.348(4)	2.339(5)
Ho···O4 (× 2)	2.471(4)	2.460(5)
<Ho···O>	2.383(5)	2.373(6)
Mn···Mn	3.00(2)	3.10(2)
Mn···Mn	2.69(2)	2.59(2)
Fe···Fe	2.956(5)	2.938(5)
Fe–O1–Fe	95.9(3)	94.0(4)
Mn–O2–Mn	100.2(9)	101.5(8)
Mn–O3–Mn	96.0(9)	94.6(9)
Mn–O3–Fe	131.5(5)	132.3(5)
Mn–O4–Fe	123.6(4)	121.4(3)

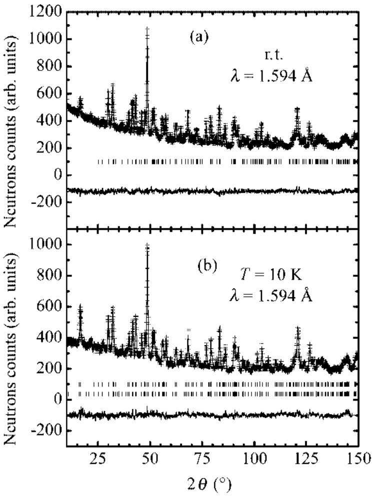

Figure 4. Comparison of the experimental (crosses), calculated (solid line) and difference (at the bottom) NPD patterns. (a) At room temperature; the tick marks correspond to the positions of the allowed Bragg reflections. (b) At T = 10 K; the first and second rows of tick marks correspond to the nuclear and magnetic reflections, respectively.

The crystallographic structure at T = 10 K has also been refined from high-resolution NPD data in the same orthorhombic space group *Pbam*. At this temperature HoFeMnO$_5$ is magnetically ordered; therefore, the magnetic contribution to the NPD pattern was taken into consideration. After including the magnetic structure described below, the refinement yielded the lattice parameters, atomic positions and discrepancy factors also included in Table 1 and Table 2; the most important interatomic distances and bond angles are listed in Table 3. As it can be observed in Table 2, the anti-site disorder between the Fe and Mn cations is very similar to that found at room temperature. The experimental and calculated NPD patterns are compared in Figure 4b.

In Figure 5, a projection of the crystallographic structure along the *c* axis is presented. Mn^{4+} cations (4*f* site) are at the centre of Mn^{4+}O$_6$ octahedra which share edges via the equatorial O2 and O3 oxygen atoms, forming infinite chains along the *c* axis. The Fe^{3+} cations (4*h* site) are coordinated to five closer neighbouring oxygen atoms in a pyramidal configuration; in the Fe^{3+}O$_5$ pyramids the O3 oxygen atom is in the axial position and the O1 and O4 oxygen atoms are in the equatorial plane. Two Fe^{3+}O$_5$ pyramids, doubly linked by O1 oxygen atoms, form a dimer unit Fe$_2$O$_{10}$. In this way, four Mn^{4+}O$_6$ octahedral chains are linked by these dimer units through the O3 and O4 oxygen atoms.

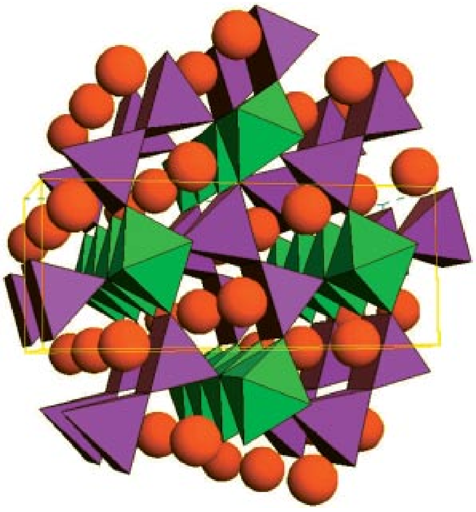

Figure 5. View of the crystallographic structure of HoFeMnO$_5$ along the *c* axis. Octahedra and tetragonal pyramids correspond to Mn^{4+}O$_6$ and Fe^{3+}O$_5$ polyhedra, respectively. The octahedra share edges, forming infinite chains along the *c* axis. The pyramids form dimer units, linking together the chains of octahedra. The spheres represent the Ho atoms.

Determination of the Magnetic Structure

The determination of the magnetic structure and the analysis of its thermal evolution was carried out from a set of NPD patterns acquired in the temperature range from 267.0 to 2.7 K. The thermal evolution of the different NPD patterns is displayed in Figure 6; upon cooling below 153 K, the intensities of some Bragg peaks start to increase, indicating the onset of a magnetic order, in good agreement with the magnetization measurements. The magnetic structure is defined by the propagation vector **k** = 0, since there are no magnetic peaks outside the permitted Bragg positions. The thermal evolution of the integrated intensity for some Bragg reflections is shown in Figure 7; in the thermal evolution of the intensity, no changes are observed that could suggest a variation in the magnetic arrangement.

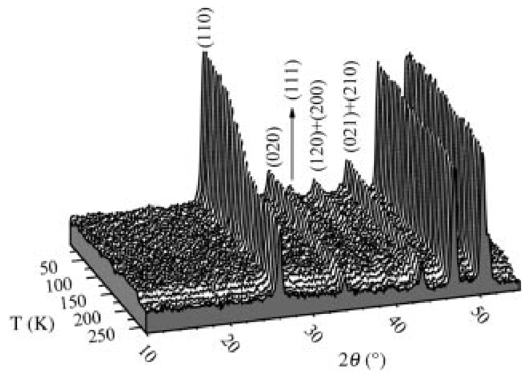

Figure 6. Thermal dependence of the NPD patterns collected with λ = 2.418 Å.

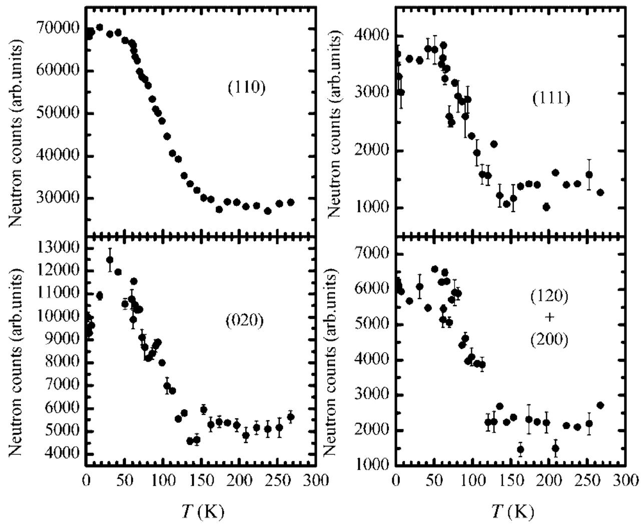

Figure 7. Thermal evolution of the integrated intensity of some magnetic reflections.

The different magnetic structure models, compatible with the crystallographic structure of the compound, have been determined from the representation analysis technique of group theory, by following the method described by Bertaut.[24] The possible magnetic structures corresponding to Mn (4*f* site), Fe (4*h* site) and Ho (4*g* site) atoms are those given in ref.[20]. The Mn atoms are labelled as 1(0,1/2,*z*), 2(1/2,0,–*z*), 3(0,1/2,–*z*) and 4(1/2,0,*z*); the notation for the Fe atoms is 5(*x*,*y*,1/2), 6(–*x*,–*y*,1/2), 7(–*x* + 1/2,*y* + 1/2,1/2) and 8(*x* + 1/2, –*y* + 1/2,1/2); the notation for the Ho atoms is 9(*x*,*y*,0), 10(–*x*,–*y*,0), 11(–*x* + 1/2,*y* + 1/2,0) and 12(*x* + 1/2, –*y* + 1/2,0).

After checking the different magnetic structure models, the solution that gives a better agreement with the experimental results corresponds to the basis vectors $(0,0,F_z)$, $(0,0,F'_z)$, and $(0,0,F''_z)$ for the Mn^{4+}, Fe^{3+} and Ho^{3+} ions, respectively. For the Fe^{3+} and Ho^{3+} cations, the moments are oriented along the positive *z* direction, whereas for Mn^{4+}cations, the magnetic moments are directed along the negative *z* direction, in a global ferrimagnetic structure. At *T* = 2.7 K the magnetic moment values for Mn^{4+}, Fe^{3+} and Ho^{3+} ions are 1.31(6), 3.20(1) and 0.36(7) μ_B, respectively (see Table 4). The good agreement between the experimental and calculated NPD patterns after the fitting of the magnetic structure at *T* = 2.7 K is shown in Figure 8; the discrepancy factors of the refinement are displayed in Table 4. A schematic plot of the ferrimagnetic order is presented in Figure 9. The thermal evolution of the magnetic moments for the magnetic ions is displayed in Figure 10; according to this figure, all the magnetic ions become ordered at the same temperature, but the magnetic moment of the Ho^{3+} cations remains nearly constant (around 0.40 μ_B) over the whole temperature range. As regards the magnetic moments of the Mn^{4+} and Fe^{3+} cations, they seem to reach saturation at around 60 K.

Table 4. Results obtained in the refinement of the magnetic structure at *T* = 2.7 K (angular range 2Θ = 8–86°). Discrep. factors: R_B = 3.9%, R_{Mag} = 9.9%, χ^2 = 3.1.

	Mn^{4+}	Fe^{3+}	Ho^{3+}
Solution	$(0,0,F_z)$	$(0,0,F'_z)$	$(0,0,F''_z)$
z Component (μ_B)	–1.31(6)	3.20(10)	0.36(7)

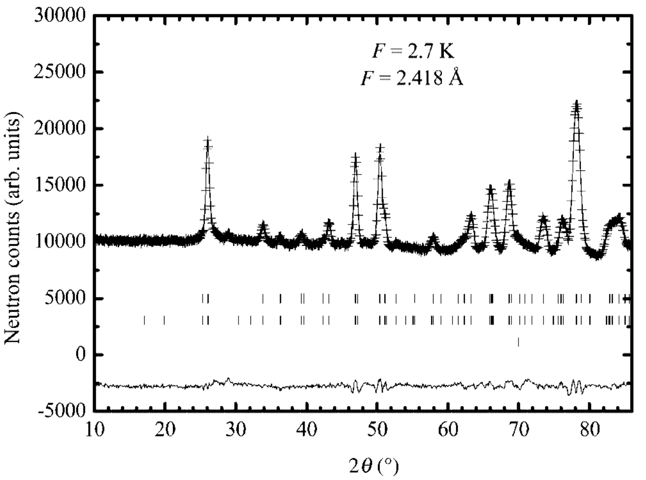

Figure 8. Experimental (crosses) and calculated (solid line) NPD patterns at *T* = 2.7 K. The first row of tick marks corresponds to the nuclear Bragg reflections and the second one to the magnetic reflections.

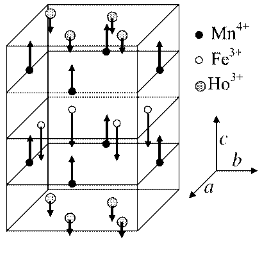

Figure 9. A view of the magnetic structure.

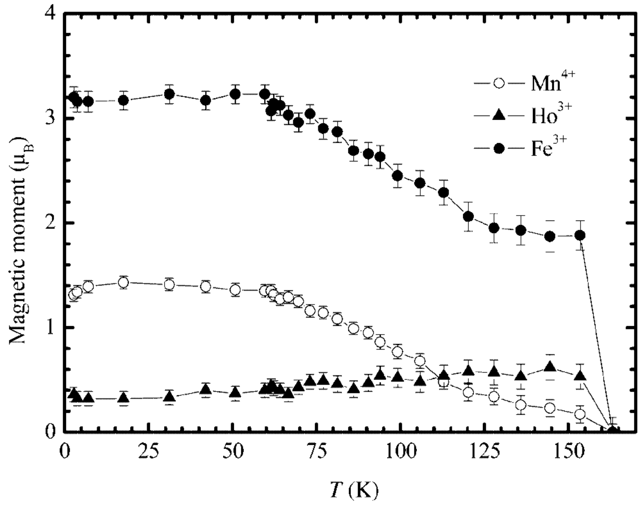

Figure 10. Thermal evolution of the module of the magnetic moments.

The thermal evolution of the lattice parameters has also been determined; as shown in Figure 11, the unit-cell volume progressively shrinks down to 130 K, and in the magnetically ordered regime, the volume remains nearly constant. The three lattice parameters *a*, *b* and *c* (not shown here) present a similar thermal variation.

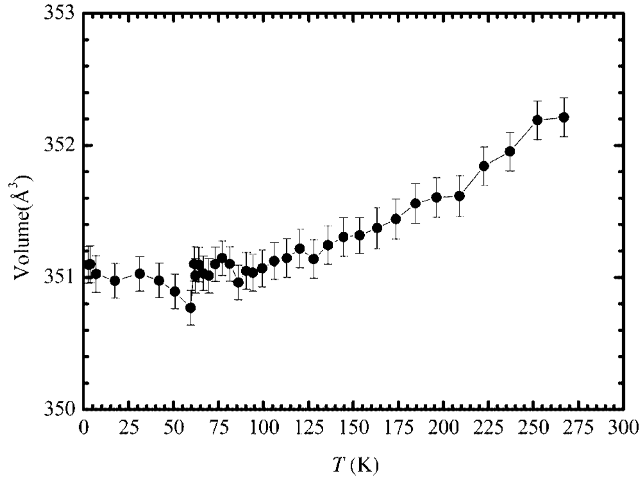

Figure 11. Thermal evolution of the volume of the unit cell.

Discussion

The analysis of the crystallographic structure of $HoFeMnO_5$ by neutron diffraction indicates that this new oxide keeps the crystallographic structure of the parent $HoMn_2O_5$ oxide[11] (space group *Pbam*). Despite the fact that the ionic radii of the Fe^{3+} and Mn^{3+}cations are very similar (0.645 Å in sixfold coordination and high-spin state[25]), some distinct features have been found both in the lattice parameters and in the interatomic distances of the $Mn^{4+}O_6$, $Fe^{3+}O_5$ and $Ho^{3+}O_8$ polyhedra. A comparison of the room-temperature lattice parameters of $HoMn_2O_5$,[11] $a = 7.2643(3)$, $b = 8.4768(3)$ and $c = 5.6700(2)$ Å, with those of $HoFeMnO_5$, shows that the substitution of the Mn^{3+} cations by Fe^{3+} gives rise to an expansion of the unit-cell parameters. The changes in the interatomic distances in the $Mn^{4+}O_6$ octahedra are not very significant; the average bond length is 1.902(2) Å in $HoMn_2O_5$ and 1.891(9) Å in $HoFeMnO_5$. In both cases the $Mn^{4+}O_6$ octahedral are flattened, because the three Mn–O distances are different; the Mn–O3 and Mn–O2 bonds in the equatorial plane correspond to the shorter and longer bonds, respectively. In the tetragonal pyramids, the substitution of Mn^{3+} by Fe^{3+} causes a shortening of the axial bond length Fe–O3 and an elongation of the equatorial bond lengths Fe–O4 and Fe–O1, with a slight average expansion of the pyramidal units: the average bond length is 1.933(3) Å in $HoMn_2O_5$ and 1.947(4) Å in $HoFeMnO_5$. The changes observed in the tetragonal pyramids cannot be related to the ionic radii, because Mn^{3+} and Fe^{3+} have the same tabulated value. The changes are very possibly linked to the Jahn–Teller character of the Mn^{3+} cations, which favour the lengthening of the axial interatomic distance in order to remove the degeneracy of the t_{2g} and e_{2g} energy levels; the Fe^{3+} cations do not show such a Jahn–Teller character. Finally, in the $Ho^{3+}O_8$ polyhedron, although some slight variations in the individual Ho···O interatomic distances are observed, the average Ho···O distances are very similar, 2.381(2) Å in $HoMn_2O_5$ and 2.383(5) Å in $HoFeMnO_5$.

The magnetic structure of $HoFeMnO_5$ is similar to the magnetic structure of the previously described members of the $RFeMnO_5$ family, with R = Y and Er; the magnetic moments within the Mn^{4+} and Fe^{3+} sublattices are ferromagnetically coupled, and the two sublattices couple antiferromagnetically, giving rise to a global ferrimagnetic structure in such a way that the magnetic unit cell coincides with the crystallographic one. In all the mentioned compounds the magnetic moments are oriented along the *z* direction. However, $HoFeMnO_5$ presents certain features that distinguish it from other members of the series containing paramagnetic R^{3+} cations, namely $ErFeMnO_5$. Firstly, the ordered magnetic moments of the Mn^{4+} and Fe^{3+} cations at 2 K, 1.31(6) and 3.20(10) μ_B, respectively, are relatively small in comparison with the theoretical values of 3 and 5 μ_B. Secondly, the ordered magnetic moment of Ho^{3+} is very small relative to the magnetic moment reached by Er^{3+} in $ErFeMnO_5$,[21] 8.59(7) μ_B; in fact, it can be said that the Ho^{3+} moments undergo a weak long-range magnetic order. The different magnetic behaviour of the Er^{3+} and Ho^{3+} sublattices is clearly exhibited by the different thermal evolution presented by the magnetic reflections (110) and (020): although in $ErFeMnO_5$[21] these magnetic reflections undergo a sharp increase below 75 K, in $HoFeMnO_5$ the integrated intensity of the mentioned reflections increase monotonically below $T_C \approx 153$ K, reaching saturation at around 50 K, much like the situation in $YFeMnO_5$.

The magnetic ordering of the Mn^{4+} and Fe^{3+} sublattices is defined by the superexchange interactions that appear between the Mn^{4+}···Mn^{4+}, Mn^{4+}···Fe^{3+} and Fe^{3+}···Fe^{3+} cations. The magnetic interactions between the Mn^{4+}···Mn^{4+}

cations are characterized by the J_1 and J_2 superexchange interactions, which are associated with the Mn^{4+}–O2–Mn^{4+} and Mn^{4+}–O3–Mn^{4+} paths, with bond angles of 101.5(8)° and 94.6(9)°, respectively, at $T = 10$ K. The Goodenough–Kanamori rules[26,27] for a 90° cation(d^3)–anion–cation(d^3) interaction indicate the presence of ferromagnetic (FM) and antiferromagnetic (AFM) interactions, the AFM interactions being mainly associated with a direct overlap of the t_{2g} orbitals of the two cations, which strongly depends on the interatomic distance between the two cations. This subtle equilibrium between AFM and FM interactions along the chains of the MnO_6 octahedra, which in the case of the parent RMn_2O_5 compounds gives rise to incommensurate magnetic structures, is clearly broken by the presence of Fe at the pyramidal positions via strong Fe–O–Fe FM interactions followed by AFM Fe–O–Mn coupling, giving rise to positive J_1 and J_2 superexchange interactions along the chains of the octahedra.

It seems reasonable to think that the strong superexchange Fe–O–Fe interactions within the dimer Fe_2O_{10} units trigger the onset of the magnetic ordering of the Fe^{3+} spins immediately below T_C. There is an abrupt change in the reciprocal dc susceptibility at 220 K, as displayed in the inset of Figure 1, which plausibly coincides with the onset of Fe–O–Fe short-range interactions. In each dimer, the two Fe^{3+} cations are linked through the O1 oxygen with a bond angle at $T = 10$ K of 94.0(4)°. We can define J_5 as the superexchange interaction across the Fe^{3+}–O1–Fe^{3+} path (Figure 12). On considering the Goodenough–Kanamori rules[26,27] for a 90° cation(d^5)–anion–cation(d^5) interaction, the coupling between the $Fe^{3+}\cdots Fe^{3+}$ cations via O1 oxygen atoms would be FM ($J_5 > 0$), in accord with Hund's rule applied to the p_x and p_y orbitals of the central O1 oxygen, forming strong σ chemical bonds with the $d_{z^2-y^2}$ orbitals of neighbouring Fe atoms.

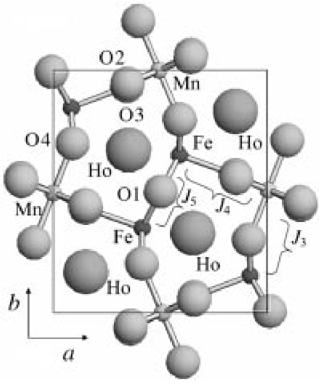

Figure 12. A view of the crystallographic structure along the [001] direction.

As it can be seen in Figure 12, the $Mn^{4+}\cdots Fe^{3+}$ interactions are characterized by the superexchange Fe^{3+}–O4–Mn^{4+} (J_3) and Fe^{3+}–O3–Mn^{4+} (J_4) paths, whose bond angles are 121.4(3)° and 132.3(5)°, respectively, at $T = 10$ K. The Goodenough–Kanamori rules[26,27] indicate that for a 180° cation(d^5)–anion–cation(d^3) interaction, the superexchange interactions are predominantly FM, whereas for a 90° bond there are FM and AFM interactions, the AFM interactions being more important. As the bond angles are closer to 90°, it seems that the superexchange interaction in the Fe^{3+}–O4–Mn^{4+} and Fe^{3+}–O3–Mn^{4+} bonds are mainly AFM ($J_3 < 0$, $J_4 < 0$). These interactions define the global AFM coupling between the Fe and Mn sublattices, giving rise to a ferrimagnetic structure.

As regards the ordering of the Ho^{3+} sublattice, the experimental results suggest that the Ho^{3+} moments are weakly polarized by the molecular field of the Fe^{3+} magnetic sublattice immediately below T_C, giving rise to FM and AFM alignments with the Fe^{3+} and Mn^{4+} sublattices, respectively. In principle, a weak direct superexchange interaction is expected between the Ho^{3+} cations via the $Ho^{3+}\cdots$O1$\cdots Ho^{3+}$, $Ho^{3+}\cdots$O2$\cdots Ho^{3+}$ and $Ho^{3+}\cdots$O4$\cdots Ho^{3+}$ paths (see Figure 12); therefore, the observed magnetic order at relatively high temperatures should be caused by the interaction with the Mn^{4+} and Fe^{3+} cations. The superexchange interactions would take place via the $Ho^{3+}\cdots$O1–Fe^{3+} (J_6), $Ho^{3+}\cdots$O4–Fe^{3+} (J_7), $Ho^{3+}\cdots$O2–Mn^{4+} (J_8) and $Ho^{3+}\cdots$O4–Mn^{4+} (J_9) paths; the interaction through the Ho$\cdots$O1–Fe path involves the indirect interaction with the two Fe^{3+} cations of the dimer. Besides, around the O1 oxygen there are two Ho atoms linked by an inversion centre and the $\mathbf{r} = \mathbf{a} + \mathbf{b}$ lattice translation; so, independently of the sign of J_6, both Ho^{3+} cations must be ferromagnetically coupled. However, according to the magnetic structure, the interactions between Ho^{3+} and the two Fe^{3+} cations of the dimer are FM; therefore, J_6 is positive. In contrast, the coupling with the Mn^{4+} cations is AFM, so J_8 and J_9 are negative. As regarding the sign of J_7 associated with the $Ho^{3+}\cdots$O4–Fe^{3+} path, it is very possible that J_7 is negative in contrast with the sign of J_6; it would contribute to the frustration of the long-range magnetic order of the Ho^{3+} sublattice. In $ErFeMnO_5$, the scenario for the Er^{3+} sublattice can be similar, but in this compound the <Er$\cdots$O> interatomic distances are slightly shorter [2.363(2) Å at room temp.], so it seems that the direct Er$\cdots$O$\cdots$Er superexchange interactions play a more important role in the establishment of the long-range magnetic order. In $HoFeMnO_5$, with longer Ho$\cdots$O interatomic distances, the participation of the direct superexchange interactions Ho$\cdots$O$\cdots$Ho in the long-range magnetic order seems to be much less important.

Conclusions

By following a singular synthesis process that includes a thermal treatment under high oxygen pressure, it has been possible to obtain $HoFeMnO_5$. The crystallographic structure, investigated by NPD, is similar to that of $HoMn_2O_5$ (orthorhombic, space group *Pbam*), and can be described as infinite chains of edge-sharing $Mn^{4+}O_6$ octahedra running along the *c* axis; the chains are corner-linked by pairs of $Fe^{3+}O_5$ edge-sharing pyramids; the Ho^{3+} cations are arranged in voids with eightfold oxygen coordination. A certain cationic disorder has been found over the 4*f* and 4*h* sites, ideally occupied by the Mn^{4+} and Fe^{3+} cations, respectively: the crystallographic formula can be rewritten as $Ho(Fe_{0.86(2)}Mn_{0.14(2)})_{4h}(Mn_{0.94(2)}Fe_{0.06(2)})_{4f}O_{4.74(10)}$. In contrast with $HoMn_2O_5$, showing elongated $Mn^{3+}O_5$ pyramids, the $Fe^{3+}O_5$ units in $HoFeMnO_5$ are flattened; this difference is ascribed to the Jahn–Teller character of the Mn^{3+} cations.

Magnetization and NPD data show that $HoFeMnO_5$ is a ferrimagnet with $T_C \approx 153$ K; the magnetic structure is characterized by $\mathbf{k} = 0$, consisting of an AFM arrangement of Fe^{3+} and Mn^{4+} spins, aligned along the *c* axis. Ho^{3+} moments become slightly polarized below T_C, ferromagnetically coupled to the Fe^{3+} sublattice and antiferromagnetically coupled to the Mn^{4+} sublattice. At $T = 2.7$ K, the magnetic moment values for the Mn^{4+}, Fe^{3+} and Ho^{3+} ions are 1.31(6), 3.20(10) and 0.36(7) μ_B, respectively. In contrast with the full long-range magnetic ordering of Er^{3+} cations in $ErFeMnO_5$, where the initial polarization of Er moments immediately below T_C is completed at lower temperatures by direct Er···O···Er interactions, in the present case it seems that the participation of direct Ho···O···Ho superexchange interactions in the long-range magnetic order is insignificant and the Ho^{3+} moments remain in a quasi-paramagnetic state down to 2 K in $HoFeMnO_5$.

Acknowledgments

We thank CICyT for the financial support of the project MAT2004-0479 and CAM for financing the project GR/MAT/0427/2004, and we are grateful to ILL for making all facilities available.

[1] Y. F. Popov, A. M. Kadomtseva, S. S. Krotov, G. P. Vorob'ev, M. M. Lukina, *Ferroelectrics* **2002**, *279*, 147.
[2] T. Kimura, T. Goto, H. Shintani, K. Ishizaka, T. Arima, Y. Tokura, *Nature* **2003**, *426*, 55.
[3] N. Hur, S. Park, P. A. Sharma, J. Ahn, S. Guha, S.-W. Cheong, *Nature* **2004**, *429*, 392.
[4] L. C. Chapon, G. R. Blake, M. J. Gutmann, S. Park, N. Hur, P. G. Radaelli, S.-W. Cheong, *Phys. Rev. Lett.* **2004**, *93*, 177402.
[5] N. Hur, S. Park, P. A. Sharma, S. Guha, S.-W. Cheong, *Phys. Rev. Lett.* **2004**, *93*, 107207.
[6] R. Valdés Aguilar, A. B. Sushkov, S. Park, S.-W. Cheong, H. D. Drew, *Phys. Rev. B* **2006**, *74*, 184404.
[7] S. Quezel-Ambrunaz, E. F. Bertaut, G. Buisson, *C. R. Acad. Sci.* **1964**, *258*, 3025.
[8] E. F. Bertaut, G. Buisson, A. Durif, A. Mareschal, M. C. Montmory, S. Quezel-Ambrunaz, *Bull. Soc. Chim. Fr.* **1965**, 1132.
[9] E. F. Bertaut, G. Buisson, A. Durif, A. Mareschal, M. C. Montmory, S. Quezel-Ambrunaz, *Bull. Soc. Chim. Fr.* **1965**, 1132.
[10] J. A. Alonso, M. T. Casais, M. J. Martínez-Lope, I. Rasines, *J. Solid State Chem.* **1997**, *129*, 105.
[11] J. A. Alonso, M. T. Casais, M. J. Martínez-Lope, J. L. Martínez, M. T. Fernández-Díaz, *J. Phys.: Condens. Matter* **1997**, *9*, 8515.
[12] G. Buisson, *Phys. Status Solidi A* **1973**, *16*, 533.
[13] G. Buisson, *Phys. Status Solidi A* **1973**, *17*, 191.
[14] A. Muñoz, J. A. Alonso, M. T. Casais, M. J. Martínez-Lope, J. L. Martínez, M. T. Fernández-Díaz, *Phys. Rev. B* **2002**, *65*, 144423.
[15] A. Muñoz, J. A. Alonso, M. T. Casais, M. J. Martínez-Lope, J. L. Martínez, M. T. Fernández-Díaz, *Eur. J. Inorg. Chem.* **2005**, 685.
[16] G. R. Blake, L. C. Chapon, P. G. Radaelli, S. Park, N. Hur, S.-W. Cheong, J. Rodríguez-Carvajal, *Phys. Rev. B* **2005**, *71*, 214402.
[17] S. Kobayashi, T. Osawa, H. Kimura, Y. Noda, I. Kagomiya, K. Khon, *J. Phys. Soc. Jpn.* **2004**, *73*, 1031.
[18] S. Kobayashi, T. Osawa, H. Kimura, Y. Noda, I. Kagomiya, K. Khon, *J. Phys. Soc. Jpn.* **2004**, *73*, 1593.
[19] L. C. Chapon, P. G. Radaelli, G. R. Blake, S. Park, S.-W. Cheong, *Phys. Rev. Lett.* **2006**, *96*, 097601.
[20] A. Muñoz, J. A. Alonso, M. J. Martínez-Lope, J. L. Martínez, *Chem. Mater.* **2004**, *16*, 4087–4094.
[21] A. Muñoz, J. A. Alonso, M. J. Martínez-Lope, J. L. Martínez, *Phys. Rev. B* **2005**, *72*, 184402.
[22] H. M. Rietveld, *J. Appl. Crystallogr.* **1969**, *2*, 65.
[23] J. Rodríguez-Carvajal, *Physica B* **1993**, *192*, 55.
[24] E. F. Bertaut, *Magnetism* (Eds.: G. T. Rado, H. Shull), Academic Press, New York, **1963**, vol. III, ch. 4.
[25] R. D. Shanon, *Acta Crystallogr., Sect. A* **1976**, *32*, 751.
[26] J. B. Goodenough, *Magnetism and the Chemical Bond*, Interscience Publishers, New York, **1963**.
[27] J. Kanamori, *J. Phys. Chem. Solids* **1959**, *10*, 87.

Received: December 4, 2006